Proceedings Paper:

Dardeno, T. orcid.org/0000-0002-0991-412X, Bull, L.A., Dervilis, N. et al. (1 more author) (2024) Transfer learning via intermediate structures. In: e-Journal of Nondestructive Testing. 11th European Workshop on Structural Health Monitoring (EWSHM 2024), 10-13 Jun 2024, Potsdam, Germany. NDT.net .

https://doi.org/10.58286/29727

EWSHM 2024
11th European Workshop on Structural Health Monitoring

Transfer learning via intermediate structures

Tina A. DARDENO[1], Lawrence A. BULL[2], Nikolaos DERVILIS[1], and Keith WORDEN[1]

[1] Dynamics Research Group, Department of Mechanical Engineering, University of Sheffield, Mappin Street, Sheffield S1 3JD, UK
[2] University of Cambridge, University of Cambridge CB3 0FA, UK
t.a.dardeno@sheffield.ac.uk

Abstract. Recent advances have been made in the field of population-based structural health monitoring (PBSHM), which seeks to share information across a population to improve inferences regarding the health states of the members. However, enabling knowledge transfer between structures with highly-disparate features (i.e., heterogeneous populations) is an ongoing challenge. The current work proposes a technique for knowledge transfer within a heterogeneous population, via intermediate structures that help bridge the gap in information between the structures of interest. The proposed technique is demonstrated using simulated, simple bridge structures.

Keywords: population-based SHM · transfer learning · geodesic flows · damage detection.

1 Introduction

Recent advances in population-based SHM (PBSHM) have been made with respect to transfer between *homogeneous* (i.e., similar or nominally-identical) structures [1, 2]; however, information sharing between structures far apart in the feature or structure space will often result in negative transfer. Therefore, a need in PBSHM is the development of techniques to facilitate *heterogeneous* transfer [3, 4]. As such, exploiting the underlying geometry of the space of structures is one exciting prospect for heterogeneous transfer learning. Conventional (linear) machine learning techniques often struggle with non-Euclidean data [5], whereas geometrical approaches [4, 6, 7] are naturally equipped to capture the complex curved manifold structure of non-Euclidean spaces. In addition, when transferring between vastly different domains or tasks, intermediate steps can allow for more gradual transitions [6–8].

To elucidate a little: one of the ideas in PBSHM is that the structures of a given population can be expressed in an abstract representation – an attributed graph – which allows them to be embedded in a metric space – a space of graphs [9]. The basic principle is that one would expect positive transfer between two structures to be more likely if they are similar. Given two structures with representations S and S', the metric space structure allows one to calculate the *distance* $d(S, S')$ between them. The fully-developed PBSHM framework would then attempt transfer, if the distance were lower than some bound ϵ_d. While the theory is not fully-developed at this point, recent work has made progress in estimating bounds for similarity which provide a probability of positive transfer [10]. At this point, an important issue arises: suppose that one wishes to transfer to a new structure S, which is data-poor, but there is no structure in the current population for which $d(S, S') \leq \epsilon_d$. Faced with this problem,an interesting possibility arises. Recalling that PBSHM does not distinguish (in its representation space), between real structures and models, one might be able to construct a model *intermediate* structure S^* for which $d(S, S*) \leq \epsilon_d$ and $d(S', S*) \leq \epsilon_d$. In this situation, one might accomplish transfer in two steps; first from S' to S^* and then from S^* to S'. Furthermore for large distances between S and S', one might design multiple intermediate structures so that transfer is enabled

https://doi.org/10.58286/29727

via a greater number of steps. It is important to note that transfer is actually carried out in the feature spaces of the structures; however, one can argue that proximity in the structure space is equivalent to proximity in the data space [4]. In transfer-learning terms, the feature spaces of S and S' are the *target* and *source* domains, respectively.

Now considering transfer as a map between data domains, geodesic flows [6, 7] are a concept from differential geometry, whereby the shortest path between two domains is learnt by exploiting the underlying geometry of the space. Gopalan *et al.* [6] introduced a geodesic flows approach to unsupervised domain adaptation (i.e., the target domain is unlabelled) for object recognition, where the source and target domains are represented as subspaces on a Grassmannian manifold. Influenced by the principle of incremental learning, the approach in [6] involves identifying potential intermediate domains between the source and target, and using a finite number of these domains to learn information about the domain changes. Later, Gong *et al.* [7] introduced the geodesic flow kernel, which instead integrates an infinite series of subspaces along the flow, for improved modelling of the domain shifts.

Making use of these concepts, a *heterogeneous* transfer approach for PBSHM is proposed herein. Using case studies that involve healthy and damaged simulated bridge structures, it is shown that transfer via *intermediate structures* can result in greater prediction accuracy compared to transferring directly between the source and desired target. Transfer learning along the chain is performed via normal-condition alignment with classification using support vector machines (SVM) first with a linear kernel, and then with the geodesic flow kernel [7].

The layout of this paper is as follows. Section 2 provides an overview of the theoretical background of the proposed work, including the geodesic flow kernel. Section 3 discusses the case studies using simulated bridge structures, with concluding remarks in Section 4.

2 Theoretical Background

Before discussing the proposed approach and associated case studies, it is useful to introduce some theory that pertains to the geometrical basis of this work, and including the equations necessary to formulate the geodesic flow kernel. For a more comprehensive discussion of geodesic flows and the geodesic flow kernel, interested readers are directed to [6, 7].

2.1 Geodesic flow kernel

The geodesic flow kernel [7], integrates all subspaces along the flow, to characterise incremental changes in geometrical and statistical properties between the source and target domains. The approach involves computing PCA subspaces and determining their appropriate dimensionality, developing the geodesic flow, constructing the geodesic flow kernel, and embedding the kernel into a kernel-based classifier [7].

Let $\mathbb{G}(\mathrm{D},\mathrm{d})$ denote the Grassmannian manifold, which is the collection of all d-dimensional subspaces. Let $\boldsymbol{S}_1, \boldsymbol{S}_2 \in \mathbb{R}^{\mathrm{D}\times\mathrm{d}}$ denote the principal component analysis (PCA) bases of the source and target, respectively. Then, let $\boldsymbol{R}_1 \in \mathbb{R}^{\mathrm{D}\times(\mathrm{D}-\mathrm{d})}$ and $\boldsymbol{Q} \in \mathbb{R}^{\mathrm{D}\times\mathrm{D}}$ define the orthogonal complement and orthogonal completion of $\boldsymbol{S}_1$, respectively. The cosine-sine decomposition of $\boldsymbol{Q}^\top \boldsymbol{S}_2$ is given by,

$$\boldsymbol{Q}^\top \boldsymbol{S}_2 = \begin{bmatrix} \boldsymbol{V}_1 & 0 \\ 0 & \tilde{\boldsymbol{V}}_2 \end{bmatrix} \begin{bmatrix} \boldsymbol{\Gamma} \\ -\boldsymbol{\Sigma} \end{bmatrix} \boldsymbol{V}^\top \tag{1}$$

where $\boldsymbol{V}_1$, $\tilde{\boldsymbol{V}}_2$, and $\boldsymbol{V}$ are orthogonal matrices that rotate/align the subspaces onto a common basis, such that $\boldsymbol{S}_1^\top \boldsymbol{S}_2 = \boldsymbol{V}_1 \boldsymbol{\Gamma} \boldsymbol{V}^\top$ and $\boldsymbol{R}_1^\top \boldsymbol{S}_2 = -\boldsymbol{V}_2 \boldsymbol{\Sigma} \boldsymbol{V}^\top$ [6, 7]. The arccosine and arcsine of matrices $\boldsymbol{\Gamma}$ and $\boldsymbol{\Sigma}$ are used to compute the principal angles, θ, respectively [6, 7]. Via the canonical Euclidean metric on the Riemannian manifold, the geodesic flow is parameterised as $\boldsymbol{\Phi} : t \in [0,1] \rightarrow \boldsymbol{\Phi}(t) \in \boldsymbol{G}(\mathrm{d},\mathrm{D})$, with the constraints that $\boldsymbol{\Phi}(0) = \boldsymbol{S}_1$ and $\boldsymbol{\Phi}(1) = \boldsymbol{S}_2$ [6, 7]. For other t, $\boldsymbol{\Psi}(t)$ can be given as [6, 7],

$$\boldsymbol{\Psi}(t) = \boldsymbol{Q} \begin{bmatrix} \boldsymbol{V}_1 \boldsymbol{\Gamma}(t) \\ -\tilde{\boldsymbol{V}}_2 \boldsymbol{\Sigma}(t) \end{bmatrix} \tag{2}$$

Assuming two D-dimensional feature vectors $\boldsymbol{x}_i$ and $\boldsymbol{x}_j$; their projections into the space defined by $\boldsymbol{\Phi}(t)$ are calculated for continuous time t from 0 to 1 [7]. These projections are then concatenated to form the infinite-dimensional feature vectors z_i^{∞} and z_j^{∞} [7]. Via the kernel trick, the inner product between these vectors gives the geodesic flow kernel, $\boldsymbol{G}$,

$$\langle z_i^{\infty}, z_j^{\infty} \rangle = \int_0^1 \left(\boldsymbol{\Phi}(t)^T \boldsymbol{x}_i\right)^T \left(\boldsymbol{\Phi}(t)^T \boldsymbol{x}_j\right) dt = \boldsymbol{x}_i^T \boldsymbol{G} \boldsymbol{x}_j \tag{3}$$

where $\boldsymbol{G} \in \mathbb{R}^{\mathrm{D} \times \mathrm{D}}$ is a positive semidefinite matrix [7]. The kernel matrix $\boldsymbol{G}$ can be written in closed form [7],

$$\boldsymbol{G} = \boldsymbol{Q} \begin{bmatrix} \boldsymbol{V}_1 & 0 \\ 0 & -\tilde{\boldsymbol{V}}_2 \end{bmatrix} \begin{bmatrix} \boldsymbol{\Lambda}_1 & \boldsymbol{\Lambda}_2 \\ \boldsymbol{\Lambda}_2 & \boldsymbol{\Lambda}_3 \end{bmatrix} \begin{bmatrix} \boldsymbol{V}_1^{\mathsf{T}} & 0 \\ 0 & -\tilde{\boldsymbol{V}}_2^{\mathsf{T}} \end{bmatrix} \boldsymbol{Q}^{\mathsf{T}} \tag{4}$$

where $\boldsymbol{\Lambda}_1$, $\boldsymbol{\Lambda}_2$, and $\boldsymbol{\Lambda}_3$ are diagonal matrices with elements [7],

$$\lambda_{1i} = 1 + \frac{\sin(2\theta_i)}{2\theta_i}, \quad \lambda_{2i} = \frac{\cos(2\theta_i) - 1}{2\theta_i}, \quad \lambda_{3i} = 1 - \frac{\sin(2\theta_i)}{2\theta_i} \tag{5}$$

The geodesic flow kernel is used in this work to facilitate transfer by embedding it into a support vector machine (SVM), as discussed in Section 3.3.

3 Case studies using simulated bridge structures

Simulated bridges were generated using finite-element analysis in MATLAB. They included a single 32-metre span, which was comprised of 62 two-dimensional beam elements, and a rectangular cross-section with a base of 5 meters and a height of 1 meter. Both ends of the span were fixed to ground. The source structure, $\boldsymbol{S}_1$, had one support located at the centre of the span, with mass M and stiffness K. The target structure, $\boldsymbol{S}_2$, had one support located at half the length of the span with mass M and stiffness K, and a second support located at three-quarters of the length of the span from the left end, also with mass M and stiffness K, as shown in Figure 1. It was predicted that $\boldsymbol{S}_1$ and $\boldsymbol{S}_2$ would be too far apart in the representation space to facilitate positive transfer. Therefore, the intent was to have a continuous set of structures along the path from $\boldsymbol{S}_1$ to $\boldsymbol{S}_2$. The set of structures was generated by moving the connection points for the second support along the span, starting at the centre of the span and ending with the second support at its final location for $\boldsymbol{S}_2$. As the second support moved away from the centre of the span, its mass and stiffness were incrementally increased from 0 (the mass and stiffness of the second support were 0 at the centre of the span, i.e., $\boldsymbol{S}_1$), to M and K, with the support at its final position. A total of 17 structures were generated.

For all structures, normal-condition datasets were generated using the first ten natural frequencies and replicating them each 100 times with added noise proportional to the frequency. To simulate damage, a lumped mass was added to the span, located between the location of the second support for S_2 and the fixed right end of the span. (The same damage location was used for each structure, where the location of the second support would not interfere.) Damage-condition datasets were then generated using the first ten natural frequencies and replicating them each 100 times, again with added noise proportional to the frequency.

3.1 Proposed Technique

Transfer from the source structure, $\boldsymbol{S}_1$, to the target structure, $\boldsymbol{S}_2$, was achieved by incrementally transferring across structures assumed to lie in an intermediate space between them. With the exception of $\boldsymbol{S}_1$, which was assumed to have fully-labelled data, each structure (including intermediates), were assumed to have some labelled normal-condition data and unlabelled damage-condition data, where the task was to correctly identify the healthy and damaged datasets. Predicted labels for each structure were then transferred across the chain, where the target for the current transfer became the source for the next, as in Figure 1. In fact, this is a type of self-training, similar to transductive methods in semi-supervised learning [11]. In the first examples discussed herein, transfer was performed using normal-condition alignment and an SVM classifier with a linear kernel. In the later examples, transfer was performed by first aligning the data, and then using an SVM classifier with a geodesic flow kernel. In each case, 1000 tests were run using randomised starting seeds for the random number generator in MATLAB, to vary both the generated datasets and training data for the classifiers. Transfer accuracy was evaluated by considering the prediction at the end of the chain, and comparing it to that when transferring directly from $\boldsymbol{S}_1$ to $\boldsymbol{S}_2$.

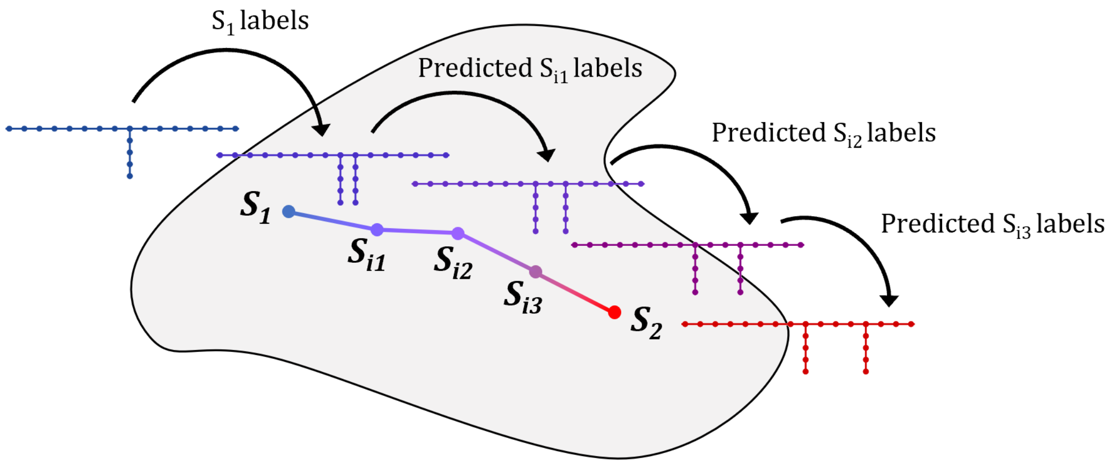

Fig. 1: Heterogeneous transfer approach via intermediate structures.

3.2 Results using the linear kernel

Using normal-condition alignment and an SVM with a linear kernel to transfer via one intermediate structure (as shown in Figure 1 as $\boldsymbol{S}_{i2}$) the prediction accuracy for damage labels at the end of the chain was higher than that when transferring directly from $\boldsymbol{S}_1$ to $\boldsymbol{S}_2$, for 96.3% of all iterations. Likewise, the average prediction accuracy for damage labels using one intermediate structure was 87.7%, compared to 39.7% for direct transfer. Using three intermediate structures (as shown in Figure 1), the prediction accuracy for damage labels at the end of the chain was higher than that when transferring directly from $\boldsymbol{S}_1$ to $\boldsymbol{S}_2$, for 99.7% of iterations. The average prediction accuracy for damage labels using three intermediate structures was 99.7%. Using the linear kernel, mean prediction accuracies, either at the end of the chain or directly from $\boldsymbol{S}_1$ to $\boldsymbol{S}_2$, are shown in Table 1. In the table, note that 'IS' refers to intermediate structure.

Table 1: Mean prediction accuracy.

Linear kernel			Geodesic flow kernel		
direct	1 IS	3 IS	direct	1 IS	3 IS
39.7%	87.7%	99.7%	66.2%	97.3%	99.8%

3.3 Results using the geodesic flow kernel

Using normal-condition alignment followed by SVM with the geodesic flow kernel, and transferring directly from $\boldsymbol{S}_1$ to $\boldsymbol{S}_2$, resulted in better transfer 72.6% of the time, and better than or equal transfer 90.9% of the time, compared to transferring directly from $\boldsymbol{S}_1$ to $\boldsymbol{S}_2$ using the linear kernel. Specifically, the average prediction accuracy for damage labels for direct transfer using the geodesic flow kernel was 66.2%. Excellent results were achieved using one intermediate structure ($\boldsymbol{S}_{i2}$ in Figure 1) and the geodesic flow kernel, with a prediction accuracy for damage labels higher than direct transfer for 73.4% of the iterations. (This is relative to direct transfer using the geodesic flow kernel. When compared to direct transfer using the linear kernel, the prediction accuracy for damage labels was higher than direct transfer for 99.4% of all iterations.) The average prediction accuracy for damage labels using one intermediate structure and the geodesic flow kernel was 97.3%. Using three intermediate structures, the transfer prediction accuracy exceeded that from direct transfer (also using the geodesic flow kernel) for 77.4% of the iterations, and 99.4% of the time compared to that from direct transfer using the linear kernel. The average prediction accuracy for damage labels using three intermediate structures was 99.8%. Using the geodesic flow kernel, mean prediction accuracies, either at the end of the chain or directly from $\boldsymbol{S}_1$ to $\boldsymbol{S}_2$, are also shown in Table 1.

4 Concluding remarks

This work proposes a novel heterogeneous transfer approach, with formulations based in differential geometry, to support PBSHM research. Using a ‘continuous’ set of simulated bridges, intermediate structures were used to bridge the gap in information between the source and target. Employing these intermediate structures resulted in overall better predictions than direct transfer.

Acknowledgements

The authors gratefully acknowledge the support of the UK Engineering and Physical Sciences Research Council (EPSRC), via grant reference EP/W005816/1. For the purpose of open access, the authors have applied a Creative Commons Attribution (CC BY) licence to any Author Accepted Manuscript version arising.

Bibliography

[1] L.A. Bull, D. Di Francesco, M. Dhada, O. Steinert, T. Lindgren, A.K. Parlikad, A.B. Duncan, M. Girolami, Hierarchical Bayesian modeling for knowledge transfer across engineering fleets via multitask learning, Comput.-Aided Civ. Inf. 38 (2023) 821–848.

[2] T.A. Dardeno, K. Worden, N. Dervilis, R.S. Mills, L.A. Bull, On the hierarchical Bayesian modelling of frequency response functions, Mech. Syst. Signal Process. 208 (2024) 111072.

[3] P.A. Gardner, L.A. Bull, J. Gosliga, N. Dervilis, K. Worden, Foundations of population-based SHM, Part III: Heterogeneous populations–mapping and transfer, Mech. Syst. Signal Process. 149 (2021) 107142.

[4] G. Tsialiamanis, C. Mylonas, E. Chatzi, N. Dervilis, D.J. Wagg, K. Worden, Foundations of population-based SHM, Part IV: The geometry of spaces of structures and their feature spaces, Mech. Syst. Signal Process. 157 (2021) 107692.

[5] M.M Bronstein, J. Bruna, Y. LeCun, A. Szlam, P. Vandergheynst, Geometric deep learning: Going beyond Euclidean data, IEEE Signal Processing Magazine 34 (2017) 18–42.

[6] G. Raghuraman, L. Ruonan, R. Chellappa, Domain adaptation for object recognition: An unsupervised approach, in: 2011 International Conference on Computer Vision, IEEE, 2011, pp. 999–1006.

[7] B. Gong, Y. Shi, F. Sha, K. Grauman, Geodesic flow kernel for unsupervised domain adaptation, in: 2012 IEEE Conference on Computer Vision and Pattern Recognition, 2012, pp. 2066–2073.

[8] A.A. Rusu, N.C. Rabinowitz, G. Desjardins, H. Soyer, J. Kirkpatrick, K. Kavukcuoglu, R. Pascanu, R. Hadsell, Progressive neural networks, 2022. arXiv:1606.04671.

[9] J. Gosliga, P.A. Gardner, L.A. Bull, N. Dervilis, K. Worden, Foundations of population-based SHM, Part II: Heterogeneous populations–graphs, networks, and communities, Mech. Syst. Signal Process. 148 (2021) 107144.

[10] A. Hughes, J. Poole, N. Dervilis, P. Gardner, K. Worden, Quantifying the value of information transfer in population-based SHM., in: Proceedings of the 42nd International Modal Analysis Conference (IMAC), Orlando, FL, 2024.

[11] M-R. Amini, V. Feofanov, L. Pauletto, L. Hadjadj, E. Devijver, Y. Maximov, Self-training: A survey, arXiv preprint arXiv:2202.12040 (2022).